nature physics

Article

https://doi.org/10.1038/s41567-022-01869-5

On-demand directional microwave photon emission using waveguide quantum electrodynamics

Received: 9 February 2022

Accepted: 4 November 2022

Published online: 5 January 2023

Check for updates

Bharath Kannan[1,2,5] ✉, Aziza Almanakly[1,2,5], Youngkyu Sung[1,2], Agustin Di Paolo[1], David A. Rower[1,3], Jochen Braumüller[1], Alexander Melville[4], Bethany M. Niedzielski[4], Amir Karamlou[1,2], Kyle Serniak[4], Antti Vepsäläinen[1], Mollie E. Schwartz[4], Jonilyn L. Yoder[4], Roni Winik[1], Joel I-Jan Wang[1], Terry P. Orlando[1,2], Simon Gustavsson[1], Jeffrey A. Grover[1] & William D. Oliver[1,2,3,4]

Routing quantum information between non-local computational nodes is a foundation for extensible networks of quantum processors. Quantum information transfer between arbitrary nodes is generally mediated either by photons that propagate between them or by resonantly coupling nearby nodes. The utility is determined by the type of emitter, propagation channel and receiver. Conventional approaches involving propagating microwave photons have limited fidelity due to photon loss and are often unidirectional, whereas architectures that use direct resonant coupling are bidirectional in principle but can generally accommodate only a few local nodes. Here we demonstrate high-fidelity, on-demand, directional, microwave photon emission. We do this using an artificial molecule comprising two superconducting qubits strongly coupled to a bidirectional waveguide, effectively creating a chiral microwave waveguide. Quantum interference between the photon emission pathways from the molecule generates single photons that selectively propagate in a chosen direction. This circuit will also be capable of photon absorption, making it suitable for building interconnects within extensible quantum networks.

Most realistic architectures of large-scale quantum processors employ quantum networks that enable the high-fidelity communication of quantum information between distinct non-local processing nodes[1]. Quantum networking enables modular and extensible quantum computation by mediating distributed entanglement between computational nodes[2,3]. There are several approaches to realizing quantum networks, including the routing of optical photons between trapped-ion modules[4], coupling emitters to photonic waveguides[5,6] or optical nanofibres[7–10], shuttling ions[11,12] or neutral atoms[13] between qubit arrays or cavity-assisted pairwise coupling between natural or solid-state artificial atoms[14–19]. Enabling non-local quantum communication is particularly relevant for qubits that are natively limited to nearest-neighbour coupling, such as two-dimensional (2D) arrays of surface-trapped ions, semiconducting qubits and superconducting qubits.

Experimental realizations of communication between superconducting qubits have typically relied on coherent coupling via

[1]Research Laboratory of Electronics, Massachusetts Institute of Technology, Cambridge, MA, USA. [2]Department of Electrical Engineering and Computer Science, Massachusetts Institute of Technology, Cambridge, MA, USA. [3]Department of Physics, Massachusetts Institute of Technology, Cambridge, MA, USA. [4]MIT Lincoln Laboratory, Lexington, MA, USA. [5]These authors contributed equally: Bharath Kannan and Aziza Almanakly. ✉e-mail: bkannan@mit.edu

https://doi.org/10.1038/s41567-022-01869-5

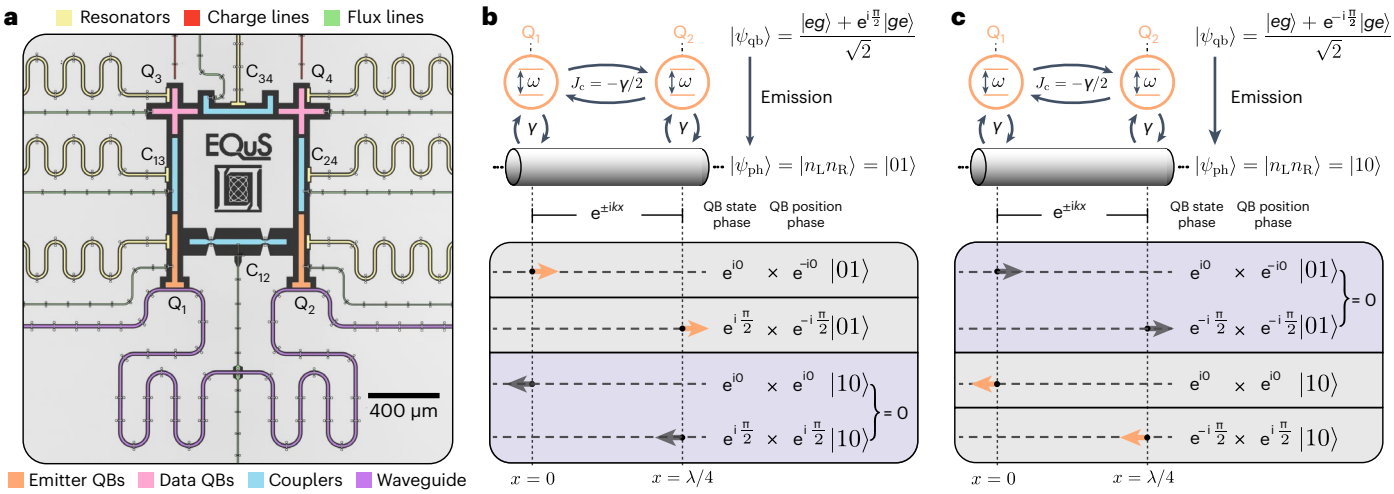

Fig. 1 | Directional emission in a waveguide QED architecture. a, A false-coloured optical micrograph of the device. The state of the data qubits (QBs) (pink) is transferred into the emitter qubits (orange) via an exchange interaction mediated by tunable couplers (blue). The emitter qubits continuously emit any population into the waveguide (purple). **b**, Schematic diagram of the two resonant emitter qubits Q_1 and Q_2 coupled to a common waveguide with equal strength γ and separated by a distance $\lambda/4$. The phase delay for photons in the waveguide is given by $e^{\pm ikx}$, where $k = 2\pi/\lambda$ is the photon wavevector and λ is the photon wavelength. The sign of this phase delay is determined by the propagation direction of the photon (+ for leftwards, and − for rightwards). An external coupler-mediated exchange interaction of strength $J_c = -\gamma/2$ is applied to fully cancel the waveguide-mediated interaction between the qubits. The four possible coherent pathways for a photon to be emitted by the qubits into the left/right-travelling modes of the waveguide are shown below. Each pathway obtains a phase from the initial state $|\psi_{qb}\rangle$ and position x of the qubit that is emitting a photon. When the qubits are initialized into $|\psi_{qb}\rangle = (|eg\rangle + e^{i\pi/2}|ge\rangle)/\sqrt{2}$, the emitted photon only propagates towards the right due to destructive interference between the left-propagating pathways. **c**, The same setup as in **b**, but with the initial qubit state $|\psi_{qb}\rangle = (|eg\rangle + e^{-i\pi/2}|ge\rangle)/\sqrt{2}$. In this case, the right-propagating pathways destructively interfere, and the emitted photon only propagates towards the left.

resonators[14–18] or itinerant photons that propagate in unidirectional waveguides[20–24]. While the former approach has achieved the highest fidelities to date, it is not easily extensible. For example, the free spectral range of the coupling resonator constrains the maximal distance between the nodes. Alternatively, itinerant photons that propagate along waveguides do not have this limitation. However, the fidelity of this approach has been limited as lossy non-reciprocal components, such as circulators, are required to prevent undesirable standing waves between nodes and render waveguides—that are naturally bidirectional—unidirectional. Instead, an architecture that uses conventional bidirectional waveguides, in conjunction with the ability to generate photons that propagate in a chosen direction, would enable both high-fidelity and high-connectivity communication within a quantum network.

Recent theoretical work has shown that superconducting circuits in a waveguide quantum electrodynamics (QED) architecture are capable of realizing such a network[25–27]. In waveguide QED, atoms are directly coupled to the continuum of propagating photonic modes in a waveguide[28]. Realizing the strong coupling regime of waveguide QED has enabled a wide range of phenomena to be experimentally observed, such as resonance fluorescence[29–32], Dicke super- and sub-radiance[33–35] and giant artificial atoms[36–40].

Importantly, the achievable strong coupling between superconducting qubits and itinerant photons enables the qubits to be used as high-quality quantum emitters[41–48]. Spatial-mode matching remains a challenge with optical emitters, such as neutral atoms near optical nanofibres[49,50]. One can instead engineer the bandgap of a photonic crystal waveguide to achieve coupling efficiencies of up to 50% with neutral atoms[51] and 99% with optical quantum dots[52]. With superconducting circuits, however, qubit-waveguide coupling efficiencies greater than 99% are readily accessible without the need for slow-light waveguides or field enhancement from cavities[35,48]. In recent years, directional emission into a waveguide has become a new sub-field of research known as chiral waveguide QED[9]. The chiral regime is naturally accessible within a nanophotonics platform, because the transverse confinement of light in optical nanowaveguides links the propagation direction of an emitted photon to the local polarization of an atom[9,53]. This effect has been leveraged to achieve directional emission of optical photons in photonic waveguides and nanofibres[5–8]. However, to the best of our knowledge, directional emission of microwave photons into chiral waveguides for integration with circuit QED systems has not yet been demonstrated experimentally.

In this work, we experimentally demonstrate on-demand directional photon emission based on the quantum interference of indistinguishable photons emitted by a giant artificial molecule.

We arrange qubits that are spatially separated along a bidirectional waveguide to form a giant artificial molecule that can emit photons in a chosen direction[25–27,54]. Effectively, we create a chiral waveguide by linking the propagation direction of an emitted photon to the relative phase of a two-qubit entangled state of the giant artificial molecule. We use quadrature amplitude detection to obtain the moments of the two output fields of the waveguide. Using these moments, we reconstruct the state of the photon and quantify its fidelity. The architecture realized here can be used for both photon emission and absorption[25], thus this demonstration is the first step towards implementing an interconnect for an extensible quantum network.

Experiment

Our device comprises four frequency-tunable transmon qubits[55] and four tunable transmon couplers[56,57] between each neighbouring qubit pair (Fig. 1a). The artificial molecule comprises two qubits, Q_1 and Q_2, each of which resonantly emits photons with a frequency of $\omega_1/2\pi = \omega_2/2\pi = 4.93$ GHz, are equally coupled to a common waveguide with strength $\gamma/2\pi = 3.2$ MHz and are spatially separated along the waveguide by a distance $\Delta x = \lambda/4$, where λ is the wavelength of the emitted photon. The remaining two qubits, Q_3 and Q_4, serve as data qubits that are not subject to direct dissipation into the waveguide. These qubits would act as the interface between a quantum processor and

https://doi.org/10.1038/s41567-022-01869-5

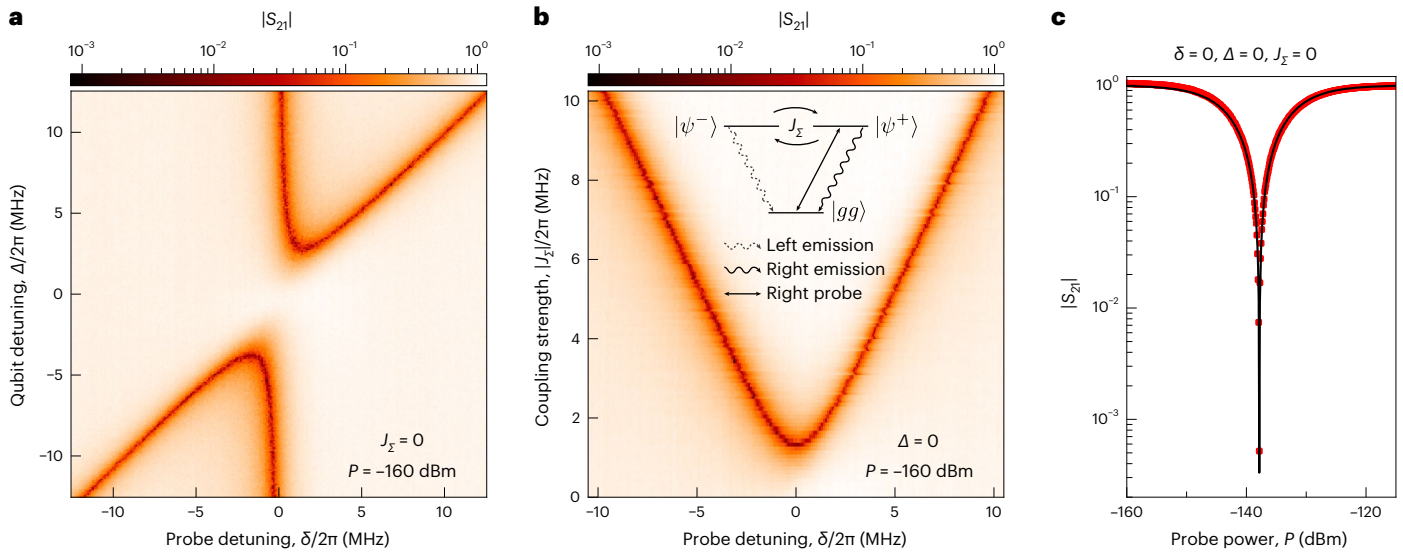

Fig. 2 | Verifying protocol conditions via elastic scattering. a, The transmittance $|S_{21}|$ of an input probe tone incident upon the two emitter qubits Q_1 and Q_2 through the waveguide. $|S_{21}|$ is plotted as a function Δ, the detuning of Q_2 from Q_1, and δ, the detuning between the probe and Q_1. When the qubits are far from resonance with each other ($\Delta > \gamma$), they will act as mirrors ($|S_{21}| \ll 1$) to the probe if the probe is resonant with either qubit ($\delta = 0, \Delta$). However, when the qubits are resonant ($\Delta = 0$), the transmittance returns to unity. **b**, $|S_{21}|$ as a function of the total coupling strength $|J_\Sigma|$ and δ while keeping Q_1 and Q_2 resonant and using the same probe power as in **a**. The level diagram of the three states $|gg\rangle$, $|\psi^+\rangle$ and $|\psi^-\rangle$ is shown as an inset ($|ee\rangle$ is ignored for weak probes). The rightwards-propagating probe used to obtain this data only couples the states $|gg\rangle \leftrightarrow |\psi^+\rangle$, and a finite exchange interaction between the emitters will couple $|\psi^+\rangle \leftrightarrow |\psi^-\rangle$. The state $|\psi^+\rangle$ can only emit a rightwards-propagating photon, and $|\psi^-\rangle$ can only emit a leftwards-propagating photon. We observe two dips in the transmission at $\delta = \pm J_\Sigma$, corresponding to the energy splitting from the hybridization of $|\psi^\pm\rangle$. When $|J_\Sigma| \to 0$, the transmission approaches unity for all δ because $|\psi^+\rangle$ is the only state that is excited, and it can only emit in the same direction (right) as the probe. This measurement is used to set $|J_\Sigma| = 0$. **c**, The measured $|S_{21}|$ (red points) as a function of the probe power with $\Delta = 0$, $\delta = 0$ and $J_\Sigma = 0$. The data agree with a fit (black curve) to a master equation simulation of the driven two-qubit system (Supplementary Fig. 3).

the emitter qubits within a node. The state of Q_3 and Q_4 can be prepared with high fidelity using a combination of single- and two-qubit gates. Photons are generated by transferring the state of the data qubits $Q_{3/4}$ to the emitter qubits $Q_{1/2}$ via an exchange interaction mediated by the couplers $C_{13/24}$.

Protocol for directional emission

The physics of the directional emission protocol is determined by the dynamics of the sub-system comprising the emitter qubits $Q_{1/2}$ and the waveguide. For $\Delta x = \lambda/4$, the master equation that determines the time evolution of the emitters is[25,28]

$$\partial_t \hat{\rho} = -\mathrm{i}\left[\hat{H}_{\mathrm{qb}} + \hat{H}_{\mathrm{c}}, \hat{\rho}\right] + \gamma \sum_j^2 D\left[\hat{\sigma}_j^-\right]\hat{\rho}, \tag{1}$$

where $\hat{\rho}$ is the density matrix of the sub-system, $D[\hat{O}] = \hat{O}\hat{\rho}\hat{O}^\dagger - \frac{1}{2}\{\hat{O}^\dagger\hat{O}, \hat{\rho}\}$ is the Lindblad dissipator, $\hat{H}_{\mathrm{qb}} = \sum_j^2 \omega_j \hat{\sigma}_j^+ \hat{\sigma}_j^-$ is the bare Hamiltonian of the emitter qubits and $\hat{\sigma}_j^\pm$ are the raising and lowering Pauli operators with $j \in \{1, 2\}$. Finally, $\hat{H}_{\mathrm{c}} = (\gamma/2 + J_{\mathrm{c}})(\hat{\sigma}_1^+\hat{\sigma}_2^- + \hat{\sigma}_2^+\hat{\sigma}_1^-)$ accounts for the exchange coupling between the qubits from two sources: a static waveguide-mediated interaction with strength $\gamma/2$ and a tunable-coupler-mediated interaction (via the tunable coupler C_{12}) with strength J_{c}. The tunability in J_{c} is used to cancel the waveguide-mediated interaction such that the emitters are decoupled from each other.

The final state of the photons emitted by Q_1 and Q_2 depends on the interference between their simultaneous emission. Specifically, when the initial state of the emitter qubits is

$$|\psi^\pm\rangle = \frac{|eg\rangle + \mathrm{e}^{\pm\mathrm{i}\frac{\pi}{2}}|ge\rangle}{\sqrt{2}}, \tag{2}$$

the node will emit a single photon that propagates either leftwards or rightwards, depending on the sign of the relative phase. To see this, consider the emitter qubits initialized to $|\psi_{\mathrm{qb}}\rangle = |\psi^+\rangle$ (Fig. 1b). There are four emission pathways from this state, each involving one of the emitter qubits, Q_1 or Q_2, releasing a photon that propagates towards the left or the right. For simplicity, we define the positions of Q_1 and Q_2 along the waveguide to be $x = 0$ and $x = \Delta x$, respectively. The pathways with a photon emitted by Q_2 will accumulate additional phases from both the relative phase $\mathrm{e}^{\mathrm{i}\pi/2}$ in $|\psi^+\rangle$ and a phase $\mathrm{e}^{\pm\mathrm{i}k\Delta x}$ from the position of Q_2 relative to Q_1. Here, $k = 2\pi/\lambda$ is the wavevector of the emitted photon, and the sign of the phase is determined by the propagation direction of the photon (+ for leftwards, and – for rightwards). These additional phases result in the total constructive (destructive) interference between the pathways that involve a photon propagating towards the right (left). Therefore, the emitted photon solely propagates to the right in the state $|\psi_{\mathrm{ph}}\rangle = |01\rangle$, where $|n_{\mathrm{L}} n_{\mathrm{R}}\rangle$ denotes the number of photons in the leftwards- and rightwards-propagating modes of the waveguide. A similar analysis for the initial qubit state $|\psi_{\mathrm{qb}}\rangle = |\psi^-\rangle$ (Fig. 1c) indicates that the emitted photon propagates towards the left in the state $|\psi_{\mathrm{ph}}\rangle = |10\rangle$ in this case.

The directional emission can be formally verified using the input–output relations for leftwards- and rightwards-propagating modes in the waveguide[28]:

$$\begin{aligned}\hat{a}_{\mathrm{L}} &= \hat{a}_{\mathrm{L}}^{\mathrm{in}} + \sqrt{\tfrac{\gamma}{2}}(\hat{\sigma}_1^- + \hat{\sigma}_2^-\mathrm{e}^{\mathrm{i}k\Delta x}),\\ \hat{a}_{\mathrm{R}} &= \hat{a}_{\mathrm{R}}^{\mathrm{in}} + \sqrt{\tfrac{\gamma}{2}}(\hat{\sigma}_1^- + \hat{\sigma}_2^-\mathrm{e}^{-\mathrm{i}k\Delta x}).\end{aligned} \tag{3}$$

Here, $\hat{a}_{\mathrm{L(R)}}^{\mathrm{in}}$ represents the input field of photons in the waveguide for the leftwards (rightwards) propagating mode. From these relations, the number of photons in either mode of the waveguide, $\langle\hat{N}_{\mathrm{L(R)}}\rangle = \langle\hat{a}_{\mathrm{L(R)}}^\dagger\hat{a}_{\mathrm{L(R)}}\rangle$, can be related directly to the state of the qubits.

https://doi.org/10.1038/s41567-022-01869-5

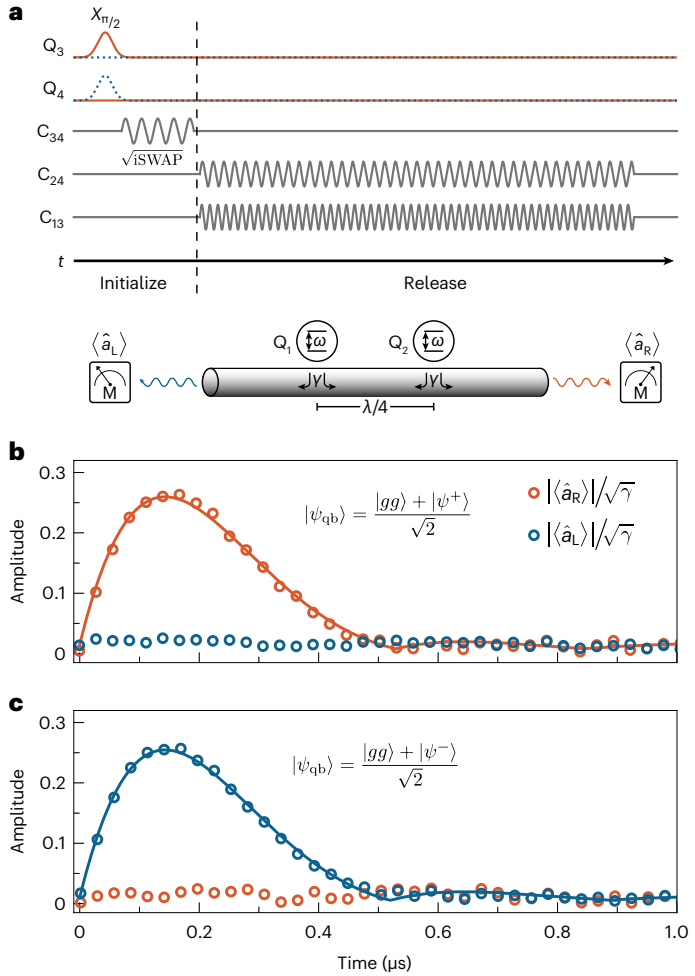

Fig. 3 | Pulse sequence and time-domain measurements. a, The pulse sequence for generating a photon. The qubit state initialization begins by exciting either Q_3 (solid orange curve) or Q_4 (dashed blue curve). These qubits are then entangled via a $\sqrt{\text{iSWAP}}$ gate by parametrically modulating the frequency of the tunable coupler C_{34} at the detuning of Q_3 and Q_4. Finally, a photon is released via a parametric exchange interaction between the data qubits $Q_{3/4}$ and the emitter qubits $Q_{1/2}$. The measurement schematic below the pulse sequence shows that the field amplitudes $\hat{a}_{L/R}$ are acquired at both outputs of the waveguide. **b**, The measured (circles) time-dependent field amplitudes for a photon emitted towards the right. The data are fit (solid curve) using the solution to the master equation (Supplementary Fig. 3). The initial state of the data qubits is $|\psi_{qb}\rangle = (|gg\rangle + |\psi^+\rangle)/\sqrt{2}$. The field amplitude of the leftwards emission channel is nearly zero. These data are averaged over 1.5×10^7 repetitions. **c**, The same measurement as in **b**, but with $|\psi_{qb}\rangle = (|gg\rangle + |\psi^-\rangle)/\sqrt{2}$ such that the emitted photon now propagates to the left.

Given that the emitters are initialized into one of $|\psi^\pm\rangle$, the interference described above is only perfect when $\Delta x = (2n+1)\lambda/4$, where n is an integer and $J_c = -\gamma/2$. The first condition ensures that the interfering emission pathways are fully in/out of phase. Additionally, it is the only spatial separation for which there is no correlated dissipation between the qubits[28], which would further disturb the interference. The second condition prevents any population transfer between the qubits during the emission process by setting the exchange Hamiltonian $\hat{H}_c$ to zero.

Device calibration for directional emission

Verifying that the ideal directional emission conditions are satisfied in the experiment is challenging. In particular, the strong and always-on dissipation into the waveguide makes it difficult to measure the strength of the coupling between the emitters, $J_\Sigma = \gamma/2 + J_c$. The typical methods, such as observations of avoided crossings in qubit spectroscopy or population exchange in the time domain, are limited in resolution when outside the strong coupling regime where $J_\Sigma < \gamma$. To go beyond this limit, we infer the value of J_Σ by measuring the elastic scattering of a weak input probe tone. Specifically, we measure the transmission amplitude S_{21} of a coherent tone as a function of the detuning between the emitter qubit frequencies, $\Delta = \omega_2 - \omega_1$, and the detuning between the probe and Q_1 frequencies, $\delta = \omega_p - \omega_1$ (Fig. 2a). When the qubits are detuned ($\Delta > \gamma$), they will each act as a mirror to single photons at their respective frequencies[29,30,35], such that there are two dips in $|S_{21}(\delta)|$. This is a consequence of the destructive interference between the probe and the forwards-propagating, out-of-phase emission of the driven qubit. Therefore, $|S_{21}|$ is suppressed for weak coherent inputs (average photon number $\ll 1$) that are resonant with either qubit.

The elastic scattering behaviour changes when the emitter qubits are resonant ($\Delta = 0$). First, given that the qubits are equally coupled to the waveguide, the input probe tone will only drive the $|gg\rangle \leftrightarrow |\psi(\phi)\rangle$ and $|\psi(\phi)\rangle \leftrightarrow |ee\rangle$ transitions, where $|\psi(\phi)\rangle = (|eg\rangle + e^{i\phi}|ge\rangle)/\sqrt{2}$. The sign of $\phi = \pm k\Delta x$ is determined by the propagation direction of the probe. Furthermore, the second transition can be ignored for low probe powers P, as it requires an appreciable population in $|\psi(\phi)\rangle$ to play a role. Therefore, if $\Delta x = \lambda/4$ and $\hat{H}_c = 0$, the state of the qubits will be driven into a mixture of only $|gg\rangle$ and one of $|\psi^+\rangle$ or $|\psi^-\rangle$, depending on the direction of the probe. However, these states can only re-emit photons in the same direction as the input, as depicted in the level diagram in Fig. 2b for a rightwards-propagating probe. This ideally results in perfect transmission, $|S_{21}(\Delta = 0)| = 1$.

The magnitude of the transmission will deviate from unity if $\hat{H}_c \neq 0$, as any population transfer between $|\psi^+\rangle \leftrightarrow |\psi^-\rangle$ will cause part of the qubit emission to propagate in the direction opposite to that of the probe. To verify this, we measure $|S_{21}(\Delta = 0)|$ as a function of $|J_\Sigma|$ (Fig. 2b). For $|J_\Sigma| > \gamma/2$, we see two dips in the transmission at $\delta = \pm J_\Sigma$, which now correspond to the hybridized energy splitting of $|\psi^+\rangle$ and $|\psi^-\rangle$. For $|J_\Sigma| < \gamma/2$, the energy splitting is within the line width of the qubits, which is set by γ. However, as described above, we observe that $|S_{21}(\delta)| \to 1$ as $J_\Sigma \to 0$. Therefore, we can use the transmission as a metric to set $J_\Sigma = 0$ despite the large decay rate γ of these qubits.

Finally, Fig. 2c shows the transmission $|S_{21}(\Delta = 0, \delta = 0, J_\Sigma = 0)|$ as a function of the probe power. Here, we clearly see $|S_{21}| \to 1$ for both low powers, as previously discussed, and high powers, where the average photon number of the probe is much greater than one and the emitter qubits are fully saturated. For intermediate powers, however, the transmission is no longer unity, because the qubits are neither fully saturated nor restricted to the zero- and single-excitation subspace. That is, the population of $|ee\rangle$ and its subsequent decay into both $|\psi^\pm\rangle$ cannot be ignored, in contrast to the simpler, low-power case. We numerically simulate the power dependence of the transmission amplitude using input–output theory. For low powers, we observe that $|S_{21}|$ slightly exceeds unity, which we attribute to impedance mismatches in our experimental set-up[58,59]. Apart from this, the resulting simulation fits well to the data in Fig. 2c, demonstrating the validity of our model. The power dependence of the transmission is similar to that of the reflection of a single emitter coupled to a semi-infinite waveguide[32,60]. In this sense, two qubits coupled to a bidirectional chiral waveguide resembles a single qubit coupled to a semi-infinite waveguide.

Photon generation and measurement

Having realized the conditions required to observe directional photon emission, we now run the full protocol using the pulse sequence shown in Fig. 3a. Rather than directly preparing the initial state of the emitter qubits into $|\psi^\pm\rangle$, which have low coherence due to their continuous dissipation into the waveguide, we instead initialize qubits Q_3 and Q_4, which have longer lifetimes. We do so by first exciting either Q_3 or Q_4 while they

https://doi.org/10.1038/s41567-022-01869-5

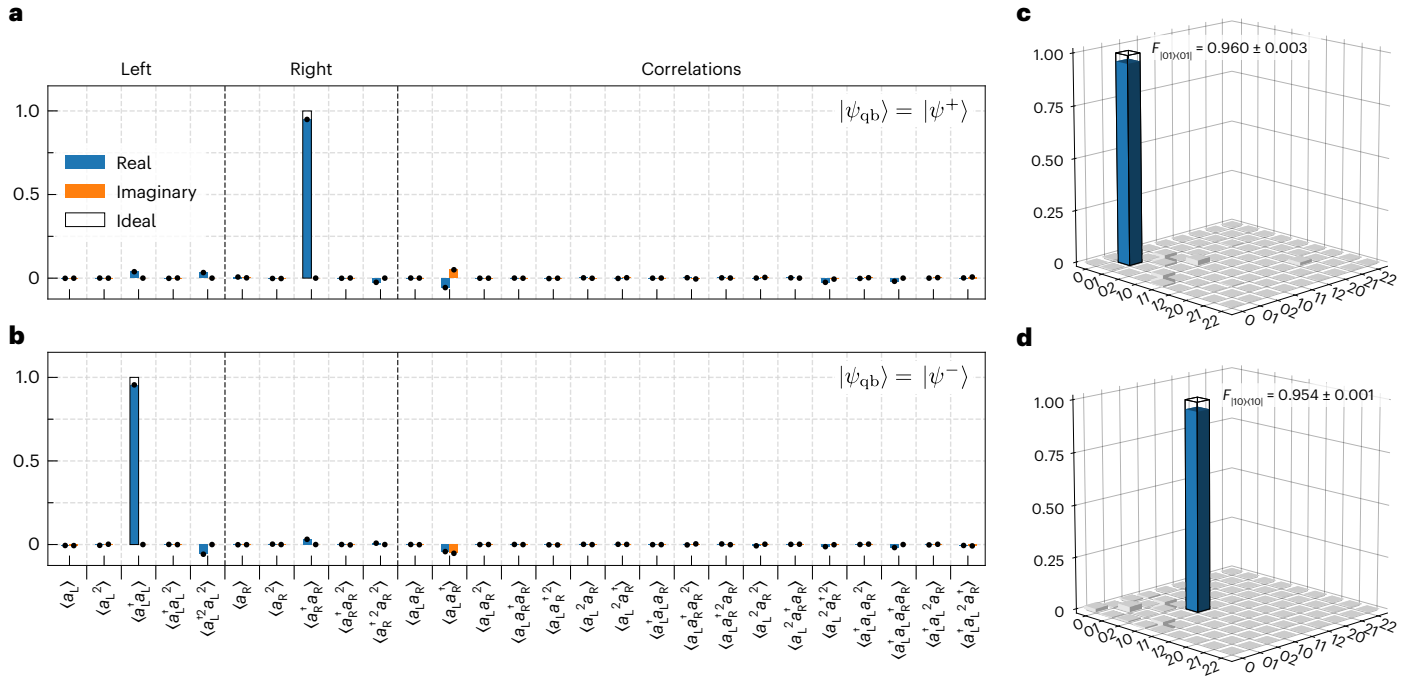

Fig. 4 | Photon state tomography. a, The moments and correlations of the left- and right-propagating channels of the waveguide up to fourth order with $|\psi_{qb}\rangle = |\psi^+\rangle$. All moments are nearly zero, except $\langle \hat{a}_R^\dagger \hat{a}_R \rangle \approx 0.95$. These data are averaged over 5×10^8 repetitions. **b**, The same as **a** but with $|\psi_{qb}\rangle = |\psi^-\rangle$. All moments are once again nearly zero, except $\langle \hat{a}_L^\dagger \hat{a}_L \rangle \approx 0.95$. **c**, The real part of the density matrix of the photon emitted to the right based on the moments shown in **a** with a state fidelity of $F_{|01\rangle\langle 01|} = 0.96 \pm 0.003$. The Hilbert space of the emitted photon is truncated to $N \leq 2$ photons. **d**, The real part of the density matrix of the photon emitted to the left based on the moments shown in **b** with a state fidelity of $F_{|10\rangle\langle 10|} = 0.954 \pm 0.001$.

are decoupled. Next, the frequency of the tunable coupler C_{34} is modulated at the detuning of this qubit pair to implement an entangling $\sqrt{\text{iSWAP}}$ gate[61]. Depending on which qubit was initially excited, the $\sqrt{\text{iSWAP}}$ gate will take the combined state of Q_3 and Q_4 to one of $|\psi^\pm\rangle$. Parametric exchange interactions mediated by the tunable couplers C_{13} and C_{24} are used to transfer the state of Q_3 and Q_4 into Q_1 and Q_2 (Supplementary Fig. 5), which simultaneously emit their excitations as photons. The interference process in Fig. 1 remains the same, but the shape of the emitted photon is now determined by both the parametrically induced coupling g_{eff} between the qubit pairs $Q_{1/2} \leftrightarrow Q_{3/4}$ and γ.

We first measure the temporal dynamics of the averaged field amplitudes $\hat{a}_{L/R}(t)$. The field amplitudes are only non-zero when there is finite coherence between the $|00\rangle$ and $|01\rangle$ or $|10\rangle$ states. Indeed, if Q_3 and Q_4 are initialized in the state $|\psi^\pm\rangle$, such that the emitted photon is in a Fock state, the field amplitude will be zero. Therefore, we initially excite Q_3 (Q_4) with a $\frac{\pi}{2}$ pulse, such that the emitted photon will be in the state with maximal coherence, $[|00\rangle + |01\rangle]/\sqrt{2}([|00\rangle + |10\rangle]/\sqrt{2})$. The photon wavepacket is now visible with maximized field amplitude (Fig. 3b,c). The amplitude of the photon is non-zero in only a single direction that is determined by the phase in the initial state of Q_3 and Q_4, a signature of the controlled directional emission. We fit this data (Supplementary Fig. 6) to obtain the effective coupling between the data and emitter qubit pairs $g_{\text{eff}}/2\pi = 1.28$ MHz.

Next, we perform photon state tomography[48,62–64] to fully reconstruct the state of the emitted photon and quantify its fidelity. We use quadrature amplitude detection of the left and right outputs of the waveguide to obtain the higher-order moments and correlations of the fields. Time-independent values of the field quadratures $S_{L/R} = X_{L/R} + iP_{L/R}$ are obtained by digitally demodulating and integrating individual records of the measured time-dependent field amplitudes. Using repeated measurements of these values, we construct a four-dimensional (4D) probability distribution $D(S_L, S_L^*, S_R, S_R^*)$ that is used to obtain the moments of S_L and S_R,

$$\langle \hat{S}_L^{\dagger w} \hat{S}_L^x \hat{S}_R^{\dagger y} \hat{S}_R^z \rangle = \int d^2 S_L d^2 S_R \, S_L^{*w} S_L^x S_R^{*y} S_R^z \, D(S_L, S_L^*, S_R, S_R^*), \quad (4)$$

where $w, x, y, z \in \{0, 1, 2, \ldots\}$. The measured signals $S_{L/R}$ are composed of both the field of interest $\hat{a}_{L/R}$ as well as noise added by the amplification chain. This additional noise is subtracted from the moments of $\hat{S}_{L/R}$, using the input–output relations for phase-insensitive amplifiers[65], to obtain the desired moments of $\hat{a}_{L/R}$[48,62,63]. These moments are normalized by the gain of the amplification chain from the qubits to the electronics used for signal acquisition.

The moments of and correlations between $\hat{a}_L$ and $\hat{a}_R$ for the photons we generate are shown in Fig. 4a,b up to fourth order. When Q_3 and Q_4 are initialized to $|\psi^+\rangle$, we obtain $\langle \hat{a}_R^\dagger \hat{a}_R \rangle \approx 1$ as the only appreciably non-zero moment, as expected for a single photon that only propagates towards the right. Similarly, we measure $\langle \hat{a}_L^\dagger \hat{a}_L \rangle \approx 1$ as the only non-zero moment for the leftwards-propagating photon emitted when the qubits are initialized to $|\psi^-\rangle$. All third- and fourth-order moments are nearly zero (with a maximum magnitude of 0.05), demonstrating the single-photon nature of the emission process.

Finally, we use these moments to obtain the density matrices of the emitted photons (Fig. 4c,d) using maximum-likelihood estimation[63,66]. Here, we truncate the Hilbert space to $N \leq 2$ photons. From these density matrices, we obtain a state fidelity of $F = 0.960 \pm 0.003$ and $F = 0.954 \pm 0.001$ for the rightwards- and leftwards-propagating photons, respectively. We observe a small, non-zero number of photons in the right (left) output of the waveguide when the qubits are initialized to $|\psi^+\rangle$ ($|\psi^-\rangle$). This infidelity results from imperfect interference between the emission pathways caused by qubit decoherence during emission and small deviations from the necessary conditions $\Delta x = \lambda/4$ and $J_\Sigma = 0$.

Discussion

Our results demonstrate that quantum interference between emitters in a waveguide QED architecture can be used to realize a directional single-photon source. While we have only performed photon generation in this work, the time reverse of the emission protocol could be used to capture photons with this same architecture if the wavepacket of the incoming photon is symmetric in time[20–22,25]. Note that the wavepacket of the generated photon can be shaped arbitrarily, in principle, by varying the time dependence of the coupling between the data and emitter qubits[20–22,25,43,67–69]. Looking forwards, we envision building a quantum network by tiling devices with the presented architecture in series and applying our protocol for both photon generation and capture. Error mitigation strategies compatible with this architecture include heralding, entanglement purification[70], teleportation with Greenberger–Horne–Zeilinger states[71] and quantum communication with W states[72]. Such a network would enable entanglement distribution and information shuttling with high fidelity in support of extensible quantum information processing.

Online content

Any methods, additional references, Nature Portfolio reporting summaries, source data, extended data, supplementary information, acknowledgements, peer review information; details of author contributions and competing interests; and statements of data and code availability are available at https://doi.org/10.1038/s41567-022-01869-5.

References

1. Kimble, H. J. The quantum internet. *Nature* **453**, 1023–1030 (2008).
2. Cirac, J. I., Zoller, P., Kimble, H. J. & Mabuchi, H. Quantum state transfer and entanglement distribution among distant nodes in a quantum network. *Phys. Rev. Lett.* **78**, 3221–3224 (1997).
3. Cirac, J. I., Ekert, A. K., Huelga, S. F. & Macchiavello, C. Distributed quantum computation over noisy channels. *Phys. Rev. A* **59**, 4249–4254 (1999).
4. Monroe, C. et al. Large-scale modular quantum-computer architecture with atomic memory and photonic interconnects. *Phys. Rev. A* **89**, 022317 (2014).
5. Söllner, I. et al. Deterministic photon–emitter coupling in chiral photonic circuits. *Nat. Nanotechnol.* **10**, 775–778 (2015).
6. Coles, R. J. et al. Chirality of nanophotonic waveguide with embedded quantum emitter for unidirectional spin transfer. *Nat. Commun.* **7**, 11183 (2016).
7. Petersen, J., Volz, J. & Rauschenbeutel, A. Chiral nanophotonic waveguide interface based on spin-orbit interaction of light. *Science* **346**, 67–71 (2014).
8. Mitsch, R., Sayrin, C., Albrecht, B., Schneeweiss, P. & Rauschenbeutel, A. Quantum state-controlled directional spontaneous emission of photons into a nanophotonic waveguide. *Nat. Commun.* **5**, 5713 (2014).
9. Lodahl, P. et al. Chiral quantum optics. *Nature* **541**, 473–480 (2017).
10. Solano, P. et al. in *Advances In Atomic, Molecular, and Optical Physics*, Vol. 66 (eds Arimondo, E. et al.) Ch. 7 (Elsevier, 2017).
11. Wan, Y. et al. Quantum gate teleportation between separated qubits in a trapped-ion processor. *Science* **364**, 875–878 (2019).
12. Pino, J. M. et al. Demonstration of the trapped-ion quantum ccd computer architecture. *Nature* **592**, 209–213 (2021).
13. Bluvstein, D. et al. A quantum processor based on coherent transport of entangled atom arrays. *Nature* **604**, 451–456 (2022).
14. Zhong, Y. P. et al. Violating bell's inequality with remotely connected superconducting qubits. *Nat. Phys.* **15**, 741–744 (2019).
15. Leung, N. et al. Deterministic bidirectional communication and remote entanglement generation between superconducting qubits. *npj Quantum Inf.* **5**, 18 (2019).
16. Chang, H.-S. et al. Remote entanglement via adiabatic passage using a tunably dissipative quantum communication system. *Phys. Rev. Lett.* **124**, 240502 (2020).
17. Zhong, Y. et al. Deterministic multi-qubit entanglement in a quantum network. *Nature* **590**, 571–575 (2021).
18. Burkhart, L. D. et al. Error-detected state transfer and entanglement in a superconducting quantum network. *PRX Quantum* **2**, 030321 (2021).
19. Ramette, J. et al. Any-to-any connected cavity-mediated architecture for quantum computing with trapped ions or rydberg arrays. *PRX Quantum* **3**, 010344 (2022).
20. Kurpiers, P. et al. Deterministic quantum state transfer and remote entanglement using microwave photons. *Nature* **558**, 264–267 (2018).
21. Axline, C. J. et al. On-demand quantum state transfer and entanglement between remote microwave cavity memories. *Nat. Phys.* **14**, 705–710 (2018).
22. Campagne-Ibarcq, P. et al. Deterministic remote entanglement of superconducting circuits through microwave two-photon transitions. *Phys. Rev. Lett.* **120**, 200501 (2018).
23. Kurpiers, P. et al. Quantum communication with time-bin encoded microwave photons. *Phys. Rev. Appl.* **12**, 044067 (2019).
24. Magnard, P. et al. Microwave quantum link between superconducting circuits housed in spatially separated cryogenic systems. *Phys. Rev. Lett.* **125**, 260502 (2020).
25. Gheeraert, N., Kono, S. & Nakamura, Y. Programmable directional emitter and receiver of itinerant microwave photons in a waveguide. *Phys. Rev. A* **102**, 053720 (2020).
26. Guimond, P.-O. et al. A unidirectional on-chip photonic interface for superconducting circuits. *npj Quantum Inf.* **6**, 32 (2020).
27. Solano, P., Barberis-Blostein, P., & Sinha, K. Collective directional emission from distant emitters in waveguide QED. Preprint at http://arxiv.org/abs/2108.12951 (2021).
28. Lalumière, K. et al. Input–output theory for waveguide qed with an ensemble of inhomogeneous atoms. *Phys. Rev. A* **88**, 043806 (2013).
29. Astafiev, O. et al. Resonance fluorescence of a single artificial atom. *Science* **327**, 840–843 (2010).
30. Hoi, I.-C. et al. Demonstration of a single-photon router in the microwave regime. *Phys. Rev. Lett.* **107**, 073601 (2011).
31. Hoi, I.-C. et al. Microwave quantum optics with an artificial atom in one-dimensional open space. *N. J. Phys.* **15**, 025011 (2013).
32. Hoi, I.-C. et al. Probing the quantum vacuum with an artificial atom in front of a mirror. *Nat. Phys.* **11**, 1045–1049 (2015).
33. Dicke, R. H. Coherence in spontaneous radiation processes. *Phys. Rev.* **93**, 99–110 (1954).
34. van Loo, A. F. et al. Photon-mediated interactions between distant artificial atoms. *Science* **342**, 1494–1496 (2013).
35. Mirhosseini, M. et al. Cavity quantum electrodynamics with atom-like mirrors. *Nature* **569**, 692–697 (2019).
36. Frisk Kockum, A., Delsing, P. & Johansson, G. Designing frequency-dependent relaxation rates and lamb shifts for a giant artificial atom. *Phys. Rev. A* **90**, 013837 (2014).
37. Kockum, A. F., Johansson, G. & Nori, F. Decoherence-free interaction between giant atoms in waveguide quantum electrodynamics. *Phys. Rev. Lett.* **120**, 140404 (2018).
38. Frisk Kockum, A. in *International Symposium on Mathematics, Quantum Theory, and Cryptography* (eds Takagi, T. et al.) 125–146 (Springer, 2021).
39. Vadiraj, A. M. et al. Engineering the level structure of a giant artificial atom in waveguide quantum electrodynamics. *Phys. Rev. A* **103**, 023710 (2021).
40. Kannan, B. et al. Waveguide quantum electrodynamics with superconducting artificial giant atoms. *Nature* **583**, 775–779 (2020).

41. Abdumalikov, A. A., Astafiev, O. V., Pashkin, Y. A., Nakamura, Y. & Tsai, J. S. Dynamics of coherent and incoherent emission from an artificial atom in a 1D space. *Phys. Rev. Lett.* **107**, 043604 (2011).
42. Hoi, I.-C. et al. Generation of nonclassical microwave states using an artificial atom in 1D open space. *Phys. Rev. Lett.* **108**, 263601 (2012).
43. Forn-Díaz, P., Warren, C. W., Chang, C. W. S., Vadiraj, A. M. & Wilson, C. M. On-demand microwave generator of shaped single photons. *Phys. Rev. Appl.* **8**, 054015 (2017).
44. González-Tudela, A., Paulisch, V., Chang, D. E., Kimble, H. J. & Cirac, J. I. Deterministic generation of arbitrary photonic states assisted by dissipation. *Phys. Rev. Lett.* **115**, 163603 (2015).
45. Pfaff, W. et al. Controlled release of multiphoton quantum states from a microwave cavity memory. *Nat. Phys.* **13**, 882–887 (2017).
46. Gasparinetti, S. et al. Correlations and entanglement of microwave photons emitted in a cascade decay. *Phys. Rev. Lett.* **119**, 140504 (2017).
47. Besse, J.-C. et al. Realizing a deterministic source of multipartite-entangled photonic qubits. *Nat. Commun.* **11**, 4877 (2020).
48. Kannan, B. et al. Generating spatially entangled itinerant photons with waveguide quantum electrodynamics. *Sci. Adv.* **6**, eabb8780 (2020).
49. Corzo, N. V. et al. Waveguide-coupled single collective excitation of atomic arrays. *Nature* **566**, 359–362 (2019).
50. Solano, P. et al. Alignment-dependent decay rate of an atomic dipole near an optical nanofiber. *Phys. Rev. A* **99**, 013822 (2019).
51. Goban, A. et al. Superradiance for atoms trapped along a photonic crystal waveguide. *Phys. Rev. Lett.* **115**, 063601 (2015).
52. Scarpelli, L. et al. 99% beta factor and directional coupling of quantum dots to fast light in photonic crystal waveguides determined by spectral imaging. *Phys. Rev. B* **100**, 035311 (2019).
53. Bliokh, K. Y., Rodríguez-Fortuño, F. J., Nori, F. & Zayats, A. V. Spin–orbit interactions of light. *Nat. Photon.* **9**, 796–808 (2015).
54. Redchenko, E. S. et al. Tunable directional photon scattering from a pair of superconducting qubits. Preprint at https://arxiv.org/abs/2205.03293 (2022).
55. Koch, J. et al. Charge-insensitive qubit design derived from the cooper pair box. *Phys. Rev. A* **76**, 042319 (2007).
56. Yan, F. et al. Tunable coupling scheme for implementing high-fidelity two-qubit gates. *Phys. Rev. Appl.* **10**, 054062 (2018).
57. Sung, Y. et al. Realization of high-fidelity CZ and ZZ-free iswap gates with a tunable coupler. *Phys. Rev. X* **11**, 021058 (2021).
58. Khalil, M. S., Stoutimore, M. J. A., Wellstood, F. C. & Osborn, K. D. An analysis method for asymmetric resonator transmission applied to superconducting devices. *J. Appl. Phys.* **111**, 054510 (2012).
59. Probst, S., Song, F. B., Bushev, P. A., Ustinov, A. V. & Weides, M. Efficient and robust analysis of complex scattering data under noise in microwave resonators. *Rev. Sci. Instrum.* **86**, 024706 (2015).
60. Scigliuzzo, M. et al. Primary thermometry of propagating microwaves in the quantum regime. *Phys. Rev. X* **10**, 041054 (2020).
61. McKay, D. C. et al. Universal gate for fixed-frequency qubits via a tunable bus. *Phys. Rev. Appl.* **6**, 064007 (2016).
62. Eichler, C. et al. Experimental state tomography of itinerant single microwave photons. *Phys. Rev. Lett.* **106**, 220503 (2011).
63. Eichler, C., Bozyigit, D. & Wallraff, A. Characterizing quantum microwave radiation and its entanglement with superconducting qubits using linear detectors. *Phys. Rev. A* **86**, 032106 (2012).
64. Lang, C. et al. Correlations, indistinguishability and entanglement in Hong–Ou–Mandel experiments at microwave frequencies. *Nat. Phys.* **9**, 345–348 (2013).
65. Caves, C. M. Quantum limits on noise in linear amplifiers. *Phys. Rev. D.* **26**, 1817–1839 (1982).
66. Chow, J. M. et al. Universal quantum gate set approaching fault-tolerant thresholds with superconducting qubits. *Phys. Rev. Lett.* **109**, 060501 (2012).
67. Yin, Y. et al. Catch and release of microwave photon states. *Phys. Rev. Lett.* **110**, 107001 (2013).
68. Pechal, M. et al. Microwave-controlled generation of shaped single photons in circuit quantum electrodynamics. *Phys. Rev. X* **4**, 041010 (2014).
69. Reuer, K. et al. Realization of a universal quantum gate set for itinerant microwave photons. *Phys. Rev. X* **12**, 011008 (2022).
70. Yan, H. et al. Entanglement purification and protection in a superconducting quantum network. *Phys. Rev. Lett.* **128**, 080504 (2022).
71. Greenberger, D. M., Horne, M. A., Shimony, A. & Zeilinger, A. Bell's theorem without inequalities. *Am. J. Phys.* **58**, 1131–1143 (1990).
72. Dür, W. Multipartite entanglement that is robust against disposal of particles. *Phys. Rev. A* **63**, 020303 (2001).

Data availability

The data that support the findings of this study are available from the corresponding author upon reasonable request.

Code availability

The code used for numerical simulations and data analyses is available from the corresponding author upon reasonable request.

Acknowledgements

The authors gratefully acknowledge D. Campbell for his contributions to the infrastructures used in this experiment, and D. K. Kim for assisting with device fabrication. This research was funded in part by the AWS Center for Quantum Computing, US Army Research Office grant no. W911NF-18-1-0411, the DOE Office of Science National Quantum Information Science Research Centers, Co-design Center for Quantum Advantage (C2QA) under contract no. DE-SC0012704 and the Department of Defense under Air Force contract no. FA8702-15-D-0001. B.K. gratefully acknowledges support from the National Defense Science and Engineering Graduate Fellowship programme. A.A. gratefully acknowledges support from the P.D. Soros Fellowship programme. Any opinions, findings, conclusions or recommendations expressed in this material are those of the author(s) and should not be interpreted as necessarily representing the official policies or endorsements of the US Government.

Author contributions

B.K. designed the experiment procedure. B.K. and A.A. designed the devices, conducted the measurements, analysed the data and wrote the manuscript. A.D.P. provided theory support. A.M. and B.M.N. performed sample fabrication. Y.S., D.A.R., K.S. and J.I-J.W. assisted with the experimental set-up. R.W. developed the custom FPGA code used to obtain the data. J.B., A.K. and A.V. assisted with the automation of the device calibration. M.E.S., J.L.Y., T.P.O., S.G., J.A.G. and W.D.O. supervised the project. All authors discussed the results and commented on the manuscript.

Competing interests

The authors declare no competing interests.

Additional information

Supplementary information The online version contains supplementary material available at https://doi.org/10.1038/s41567-022-01869-5.

Correspondence and requests for materials should be addressed to Bharath Kannan.

Peer review information *Nature Physics* thanks Giuseppe Calajò, Mathieu Juan and the other, anonymous, reviewer(s) for their contribution to the peer review of this work.